Journal of Hazardous Materials 492 (2025) 138123

Contents lists available at ScienceDirect

Journal of Hazardous Materials

journal homepage: www.elsevier.com/locate/jhazmat

Eco-friendly kappa-carrageenan-nano zerovalent iron hydrogel water and wastewater purification

Rokhsare Kardani, Sudesh Yadav, Ali Altaee [*], Lilyan Alsaka, John Zhou

Centre for Green Technology, School of Civil and Environmental Engineering, University of Technology Sydney, 15 Broadway, NSW 2007, Australia

HIGHLIGHTS

- kC membranes were prepared with 0.5–2 %wt/v nZVI and crosslinked with PEI for leachate treatment.
- nZVI-kC membranes achieved 98 % and 90 % rejection of Mg^{2+} and Na^{+} ions.
- The membranes maintained 98 % rejection of heavy metals from leachate in multiple cycles.
- The nZVi-kC recovered 68 % and 66 % of lead and lithium from leachate at the end of the experiments.

GRAPHICAL ABSTRACT

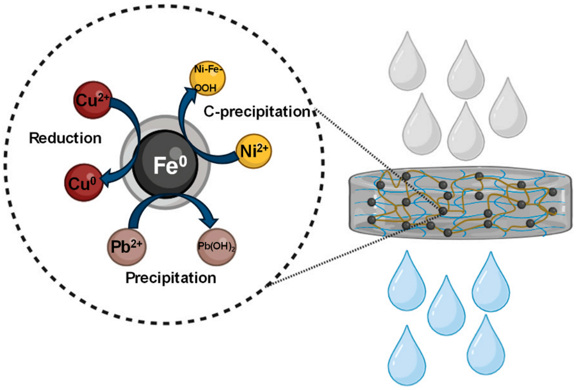

ARTICLE INFO

Keywords:
Membrane
Hydrogel
Lithium
Heavy metals recovery
Filtration

ABSTRACT

Sustainable water management is crucial for reducing environmental impact, improving public health, and contributing to the United Nations' Sustainable Development Goals (SDGs). This study introduces a novel hydrogel composite membrane for wastewater treatment and desalination. The membrane was fabricated by cross-linking kappa-carrageenan (κC) with nano-zerovalent iron (nZVI) using polyethyleneimine (PEI) to produce a porous structure hydrogel membrane of high water flux and contaminant rejection via adsorption and reduction processes, leveraging the properties of kappa carrageenan and nZVI. Experiments showed an increased water flux and rejection rate for the hydrogel membrane by increasing the pressure from 10 psi to 30 psi. In initial tests with 2 g/L of NaCl or $MgSO_4$, the membrane exhibited 98 % rejection of divalent Mg^{2+} ions and 90 % rejection of Na^{+} ions at 30 psi and 17.98 L/M2H water flux. The hydrogel's contaminant separation mechanisms involve a combination of size exclusion, electrostatic repulsion, and hydrophilic-hydrophobic polarity rejection. Leachate wastewater treatment by the membrane achieved 11 L/m^{2}h water flux at 30 psi and an outstanding rejection rate of more than 98 % for divalent ions, such as Li^{+}, Pb^{2+}, Cd^{2+}, Co^{2+}, and Cu^{2+}, and 61 % rejection of organic matter of 165.68 mg/L initial concentration. Due to membrane fouling, the water flux decreased in the second and third filtration cycles, while membrane rejection remained unchanged. The dead-end filtration mode facilitated metal ions recovery at the end of the experiments, recording 68.32 % and 66.31 % recovery for lead

---

[*] Corresponding author.
E-mail address: ali.altaee@uts.edu.au (A. Altaee).

https://doi.org/10.1016/j.jhazmat.2025.138123
Received 2 November 2024; Received in revised form 11 February 2025; Accepted 30 March 2025

and lithium ions. This novel hydrogel provides a promising and sustainable solution for water purification and valuable heavy metals recovery from solutions to support the circular economy.

1. Introduction

Water is essential for economic, social, and cultural development, but it faces significant challenges due to increasing global demand from urbanization and industrialization. Poor water management, inadequate infrastructure, pollution, and climate change contribute to widespread water scarcity [1–3]. Industrial activities, consuming about 22 % of the world's water, are a major source of water pollution. They release nearly 80 % of global wastewater untreated, contaminating water bodies and posing severe risks to the environment, human health, and aquatic life [3,4]. Among pollutants, heavy metals are especially concerning because of their toxicity and ability to enter the food chain through plant absorption and ingestion by fish [4,5]. Human activities, such as electroplating and metal smelting, are the primary sources of heavy metal pollution, necessitating effective wastewater treatment to reduce these contaminants to safe levels before environmental release [5,6]. Water scarcity has driven many communities to seek reliable access to clean water, increasing the demand for advanced water treatment techniques as water sources diminish. Seawater desalination and reuse of wastewater reuse are key strategies to enhance water availability, given that the majority of the global water resource is seawater [7]. Membrane separation technology, widely adopted across industries like petroleum, food, pharmaceuticals, and electronics, has become a prominent solution because of its benefits, such as minimal energy usage, scalability, and fouling resistance [7–10]. Among membrane materials, polymeric substances have received significant attention, with hydrogels gaining recognition as a potential category of polymeric membranes for water treatment [11,12].

Hydrogels consist of three-dimensional frameworks of hydrophilic polymers capable of absorbing significant quantities of water and come in various forms like injectable hydrogels, scaffolds, and hydrogel membranes (HM) [11–13]. During swelling, they maintain structure through physical or chemical cross-linking, with physical cross-linking creating temporary bonds and chemical cross-linking forming permanent ones [14]. Hydrogels are responsive to environmental changes, which makes them useful in medicine, tissue engineering, and wastewater treatment [11,13]. They offer benefits such as high water absorption, porosity, and ease of fabrication from natural or synthetic polymers [11,13,15]. Natural hydrogels like alginate, chitosan, and carrageenan are eco-friendly but may have mechanical strength issues, while synthetic hydrogels like PAA and PVP are widely used [16]. Optimal hydrogel membranes for filtration and desalination must be resistant to fouling, be selective, and be stable [17]. Carrageenan is a hydrophilic sulfated galactan derived from red marine algae and known for its water-absorbing properties. It is employed in bioadsorbent materials as a result of its ability to adsorb pollutants [18]. The kappa-carrageenan (κC) has strong gel-forming abilities, making it useful in various industries. However, humid conditions can limit its mechanical strength, necessitating blending with other biopolymers or the addition of nano-reinforcing fillers [19,20]. Yadav et al. [21] coated commercial UA-60 NF membranes using a κ-CGN-GO solution to enhance salt rejection and antifouling characteristics. Optimal coating conditions were determined, resulting in membranes with enhanced selectivity and reduced fouling. The κC-GO coating showed a rejection of 95 % for $MgSO_4$ and 23 % for NaCl. Soomro et al. [22] fabricated a composite membrane for saline water purification through the functionalization of GO surface with arginine amino acid. The membrane achieved 98 % rejection of NaCl, 99.8 % for $MgCl_2$, and 100 % for methylene blue and rhodamine B. In another work, Shaikh et al. [23] prepared a GO membrane crosslinked by silk fibroin for water purification. With a water permeance of 280 $L/m^2h.bar$, the fibroin-GO membrane rejected more than 99 % of dyes, including methylene blue and brilliant blue G and about 10 % of Cu^{2+}. Ibrar et al. [24] developed a biodegradable, gravity-driven κ-Carrageenan-vanillin hydrogel designed for treating landfill leachate wastewater, tackling issues related to membrane fouling, energy demands, and brine management. This hydrogel, synthesized with an average pore size of 2.58 ± 0.5 nm, exhibited high water flux and effective rejection of contaminants, including heavy metal ions and divalent ions. It achieved average rejection rates of 42 ± 5 % for sodium chloride, 78 ± 5 % for copper, and 72 ± 5 % for magnesium ions. This approach provides a cost-effective and scalable solution for landfill leachate treatment without the need for high pressures or external energy. nZVI is another nanoparticle used for treating heavy metal-contaminated wastewater. It features a metallic iron core, which offers reducing capabilities, and an iron oxide shell that attracts and adsorbs ions. These roles enable nZVI to remove oxyanions, e.g., As^{5+}, Cr^{4+}, Cu^{2+}, Zn^{2+}, Cd^{2+}, Pd^{2+}, and Ni^{2+}, with benign byproducts that pose minimal environmental risks [25]. PEI, a polyamine with multiple amine groups, has a strong chelation ability for heavy metal ions. However, because of its high water solubility, PEI requires cross-linking or integration into other matrices to function effectively as an adsorbent. Efficient removal of heavy metal ions from wastewater is enabled by hybridizing PEI with polymers, inorganic matrices, or biopolymers [26,27]. PEI possesses numerous amine groups that engage in electrostatic interactions with sulfate groups of κC, creating a flexible and resilient hydrogel with enhanced mechanical strength.

In this study, kappa Carrageenan (κC)- nano Zero Valent Iron (nZVI)-Polyethyleneimine (PEI) hydrogel membranes were prepared for wastewater treatment and water desalination. The fabricated membranes were crosslinked with PEI to enhance stability and control swelling. Incorporating nZVI will enhance membrane mechanical strength and heavy metal removal. The research questions are: i) what is the effect of nZVI incorporation in κC on the hydrogel membrane water flux and rejection? And ii) will the rejection rate and water flux of the hydrogel be affected in multiple filtration cycles? Experiments optimized the concentration of nZVI within the κC matrix to balance between maximizing permeability and maintaining selectivity. The hydrogel membrane stands out due to its synergistic combination of κC, nZVI, and PEI to enhance its mechanical strength and capability for heavy metal removal. The membrane maintained outstanding selectivity even after multiple filtration cycles, offering long-term performance under low pressure, making it an energy-efficient filtration option. Besides, it enables the recovery of valuable and rare metal ions in the solution and contributes to the circular economy. For the membrane preparation, deionized water was utilized to synthesize the composite hydrogels. Experimental work measured water contact angle, zeta potential, swelling, shear stress, and viscosity of the fabricated membranes. In addition to pure water flux, the membranes' performance was assessed by testing their rejection capabilities for 2 g/L solutions of sodium chloride (NaCl) and magnesium sulfate ($MgSO_4$) under low pressure. Real leachate wastewater was used to test the effectiveness of the fabricated membranes for heavy metal rejection and potential recoveries of valuable ions, such as Li^{+}, Cr^{3+}, Pb^{2+}, Cd^{2+}, Co^{2+}, Zn^{2+}, Pb^{2+}, and Cu^{2+} for reuse in a circular economy.

2. Materials and methods

2.1. Materials

All chemicals employed in this study were of analytical grade and were utilized in their original form without any modification. κC (sulfated plant polysaccharide) and PEI, branched (average molecular weight 25000 g/mol), were purchased from Sigma-Aldrich (Australia). Nano zerovalent iron nanoparticles (nZVI) having a molecular weight of 55.85 g/mol were purchased from NanoIron Future Technology. The wastewater examined was sourced from landfill leachate at the Hurstville Golf Centre (Sydney). The landfill wastewater was kept in a refrigerator to prevent changes in its composition. Table 1 summarizes the characteristics of the landfill leachate wastewater utilized in this investigation. Additionally, in specific experiments to evaluate rejection rates, analytical grade sodium chloride (NaCl) and magnesium sulfate ($MgSO_4$) from Sigma-Aldrich were utilized. All metal salts were dissolved in deionized (DI) water for these experiments. A cellulose acetate (CA) filter paper featuring a pore size of 0.45 μm was applied as the supporting layer for the hydrogel filter (Thermo Fisher Scientific, Sartorius Stedim Biotech GmbH, Germany). The selection of CA as a support material is due to its good mechanical strength, chemical stability, and hydrophilicity, which allows good interaction with the hydrogel. 0.45-micron pore size, the CA support layer will facilitate water permeation and prevent hydrogel penetration. The hydrogel was deposited onto the support layer in a filtration column intended for water treatment applications.

2.2. *Hydrogel membrane preparation and performance studies*

The κC hydrogel is formed by dissolving 3 % wt/v of κC powder in deionized water at 60°C, allowing it to mix using a magnetic stirrer for three hours to achieve a uniform gel-like solution. Typically, κC dissolves within the range of 60–80°C. The 3 % concentration was selected based on its proven efficacy in prior studies [24]. The nZVI dispersion and uniform distribution throughout the hydrogel were optimized by adjusting the mixing time to 1 hour at 40°C and 600 rpm. Subsequently, the nZVI powder with varying concentrations of 0.5, 1, 1.5, and 2 % wt/v was introduced to the κC solution and blended for one hour. In another container, 1 % wt/v of PEI was prepared by dissolving it in DI water and simultaneously stirring on a magnetic stirrer to achieve a homogeneous mixture for a 15-minute. 1 mL of PEI was added to each 100 mL of the κC-nZVI solution and blended (Fig. 1). Due to its amine ($-NH_2$) groups, cationic PEI strongly interacts with the κC hydrogel through electrostatic interaction, creating a dense network that reduces the hydrogel swelling. Table 2 displays the composition of all prepared membranes.

The as-prepared hydrogel was applied onto a cellulose acetate filter paper featuring a pore size of 0.45 μm to serve as a support layer for the membrane. Experimental procedures were conducted utilizing an Osmosis Inline DIY Fill Tube measuring 26 cm in height and made of PC material (Fig. 1) to enable visual monitoring, featuring a filtration area of 0.00049 m^2. In the filtration setup, the support layer and the membrane were securely positioned at the base of the filtration column, allowing 10–15 minutes for settling under a low pressure of 10 psi. Subsequently, pure water was gradually introduced into the column for filtration. Careful attention was paid throughout the filtration process to prevent abrupt water flow from impacting the hydrogel, which could distort it and compromise its effectiveness. The flux was measured at different pressures of 10, 20, and 30 psi. The careful control of feed pressure between 10 and 30 psi in the filtration tests ensured the integrity of the hydrogel, which is a common challenge in hydrogel membranes. The flux and contaminant rejection of the feed solution were determined using analytical instruments.

Table 1
Wastewater characteristics.

Parameter	Value
Appearance	Light brown colour
Total Organic Carbon (TOC)	165.68 ± 5 mg/L
pH	7.41
Total dissolved Solids	3200 ± 100 mg/L
Conductivity	3.4 ± 0.15 mS/cm
Turbidity	29 ± 3 NTU
Mg	29.02 ± 3 mg/L
Ca	28.55 ± 2 mg/L
Cd	1.641 ± 2 mg/L
Pb	1.71 ± 3 mg/L
Al	1.785 ± 1 mg/L
Cr	1.783 ± 1 mg/L
Mn	1.843 ± 2 mg/L
Li	2.074 ± 2 mg/L
Na	52.3 ± 3 mg/L
K	46.5 ± 5 mg/L
Co	1.72 ± 3 mg/L
Ni	1.682 ± 1 mg/L
Cu	1.764 ± 1 mg/L
Zn	1.874 ± 3 mg/L

Consecutive filtration cycles were conducted to evaluate membrane durability and performance over time. All experiments were conducted a minimum of three times to validate the findings. Flux was calculated through Eq. 1:

$$J = \frac{W}{1000 * A * t} \tag{1}$$

Contaminant rejection was assessed through Eq. 2:

$$R = (1 - \frac{C_{permeate}}{C_{feed}}) * 100 \tag{2}$$

In Eq. 3, $C_{permeate}$ represents the concentration of contaminants present in the permeate solution. (measured via ICP-MS analysis), while Cfeed represents the initial concentration of these contaminants in the feed solution.

2.3. *Lithium and lead recovery*

Lead poses an environmental threat at high concentrations, while lithium is a rare metal that has commercial value due to its incorporation in lithium batteries. At the end of the experiments, the membrane was dissolved in a 0.1 M hydrochloric acid (HCl) solution to recover metals from the composite hydrogel after leachate wastewater treatment. The mixture was shaken at 150 rpm for 48 hours at room temperature to ensure thorough dissolution. Afterward, the solution was centrifuged at 10,000 rpm for a 15-minute to separate any remaining solids. A liquid sample was collected and analyzed using ICP-MS to quantify the metal content. The recovery efficiency was calculated using the following equation:

$$R(\%) = \left(\frac{C_{recovered}}{C_{initial}}\right) \times 100 \tag{3}$$

$C_{recovered}$ is the concentration of metals recovered after dissolution, and $C_{initial}$ is the concentration of metals initially captured by the membrane. $C_{initial}$ was determined by analyzing the metal concentration in the leachate wastewater before treatment and calculating the total amount adsorbed by the membrane based on the difference between the feed and permeate concentrations. The results from the ICP-MS analysis were used to determine both $C_{recovered}$ and $C_{initial}$.

2.4. *Analytical methods*

Functional group analysis of the prepared hydrogels was conducted using Fourier Transform Infrared Spectroscopy (FT-IR). This analysis utilized a Thermo Scientific Nicolet spectrometer with an optical resolution of 0.9 cm^{-1}, connected to an IR microscope from Thermofisher, Sydney (Australia). Before analysis, all samples underwent drying in an oven at 80°C for 3 hours. The FT-IR analysis covered a wavenumber range from 4000 to 500 cm^{-1}. Each scan was repeated three times, and the final spectra were obtained by averaging these results.

Surface morphology was analyzed using a Field Emission Scanning Electron Microscope, FESEM (Zeiss EVO LS15 SEM (Zeiss, Sydney,

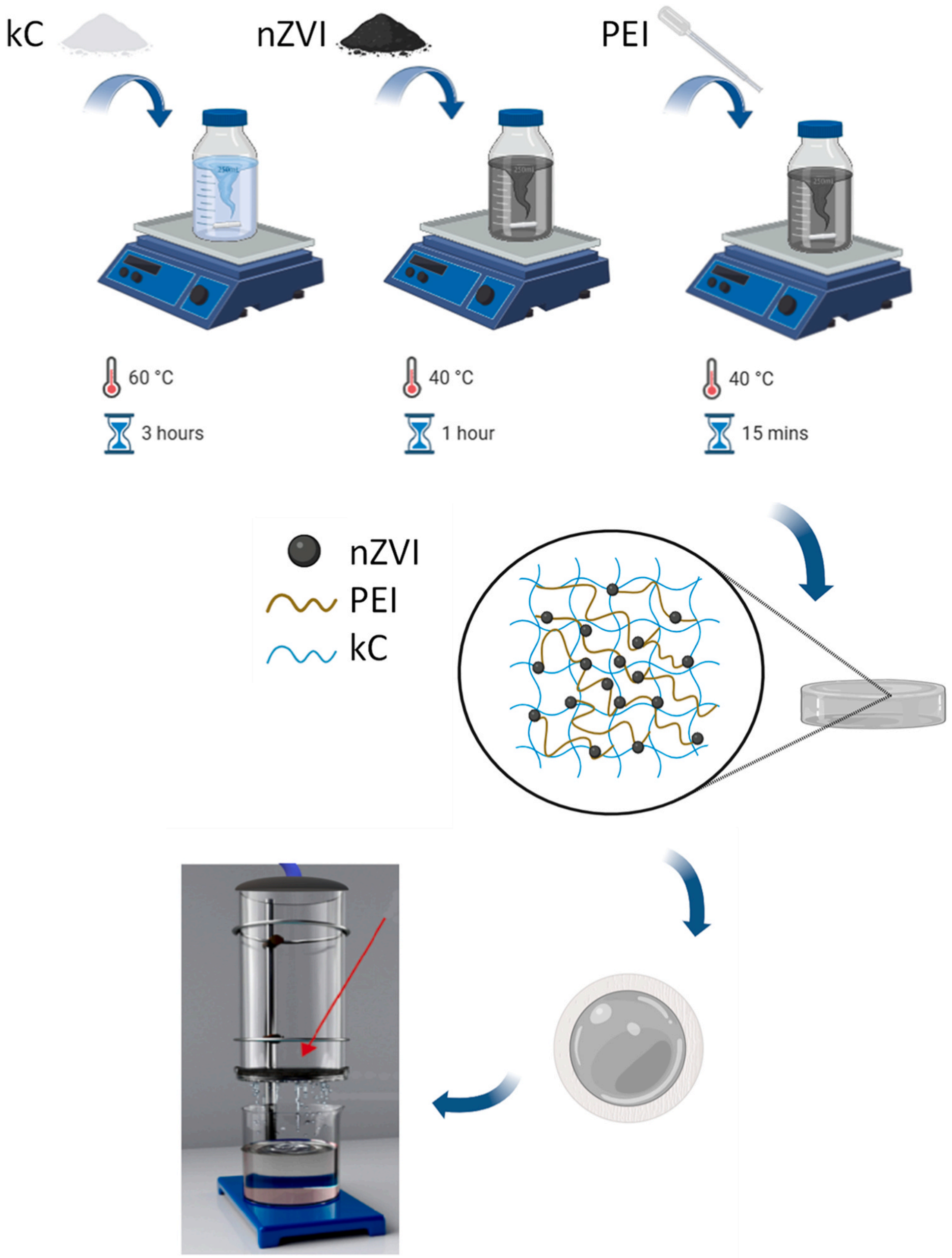

Fig. 1. Composite hydrogel preparation and a schematic of filtration setup.

Table 2
Compositions of various hydrogel membranes.

No.	Membrane	κC (% wt/v)	nZVI (% wt/v)	PEI 1 % wt/v (aq sol, mL)	Thickness (cm)
1	κC-ZVI0.5	3	0.5	1	0.5
2	κC-ZVI1	3	1	1	0.5
3	κC-ZVI1.5	3	1.5	1	0.5
4	κC-ZVI2	3	2	1	0.5
5	κC-ZVI2 *	3	2	1	0.25

Australia)). Equipped with Energy-Dispersive X-ray Spectroscopy, EDAX (Bruker SDD XFlash 5030 detector (Zeiss, Australia)). Before FESEM analysis, the membranes were fully dried and covered with a conductive thin film to avoid charging, and imaging was conducted at 10 kV. SEM analysis was complemented with cross-sectional imaging.

X-ray diffraction (XRD) analysis was performed using a Bruker D8 Discover diffractometer with Cu Kα radiation ($\lambda = 1.5406$ Å). The membranes were analyzed in dried membrane form over a 2θ range of 10° to 80°. Interlayer spacing (d-spacing) was calculated using Bragg's equation.

Samples from both the feed and filtered solutions were assessed for ion concentration through ICP-MS (Inductively Coupled Plasma Mass Spectrometry) by Agilent Technologies. The samples' total organic carbon (TOC) levels were determined with the help of a TOC analyzer from Shimatzu, Japan. The rheological properties of the membranes were evaluated with a rotating shear rheometer to evaluate the material's mechanical strength.

Measuring the water contact angle (WCA) allowed for the evaluation of the membrane surface's wettability. This study employed the sessile drop technique to determine the WCA using Kyowa Interface Science, Chennai, India. Each sample's WCA was measured in three different spots, and the average value, along with the error margin, was recorded.

The electrical charge present on the surface of the membranes was determined using conducting zeta potential (ζ) measurements at a neutral pH in water.

Further analysis of the hydrogel included water content evaluation and analysis of swelling properties. Hydrogel slices with a thickness of 1 cm underwent water uptake and swelling tests under neutral pH conditions. The water uptake (WU) of the membranes was calculated using Eq. 4:

$$\mathrm{WU} = \frac{(\mathrm{W}_2 - \mathrm{W}_1)}{\mathrm{W}_1} * 100 \tag{4}$$

Water uptake (WU) was measured using pre-dried membrane pieces, each cut to dimensions of 3 × 3 × 1 cm. These hydrogel pieces were oven-dried at 80 °C for 3 hours, and the dry weight (W_1) was recorded. After immersing the pieces in distilled water for 24 hours at room temperature, they were weighed following moisture removal (W_2), and water uptake was determined using Eq. (4). Three samples were tested, with average results recorded. Additionally, the swelling degree (SD) of the hydrogel was assessed to gauge its resistance to swelling. The initial weight of the hydrogel (W_i) was taken, and it was immersed in DI water for 2 hours. The final weight (W_f) was then taken, and the swelling degree (SD) was calculated using Eq. 5:

$$SD = \frac{(W_f - W_i)}{W_i} * 100 \tag{5}$$

The porosity of the hydrogel membrane was measured by cutting the membrane into small pieces, 3 × 3 × 0.5 cm, and immersed in distilled water for 18 hours. Afterward, the membrane pieces were gently removed, and any excess water was blotted off. The wet weight (W_{wet}) was then recorded. The membranes were oven-dried at 80°C for 3 hours and then weighed again to measure the dry weight (W_{dry}). The porosity was calculated using Eq. 6:

$$\mathrm{p}\% = \frac{\mathrm{W}_{wet} - \mathrm{W}_{dry}}{\mathrm{A} \times \mathrm{l} \times \rho} \tag{6}$$

A is the membrane surface area (cm^2), l is the thickness (cm), and ρ is the water density (1 g/cm^3). (Table 3)

The average pore radius r was then calculated using pure water flux and the membrane porosity with Eq. 7:

$$\sqrt{\frac{(2.9 - 1.75\mathrm{p}) \times (8 \times \mathrm{lQ}\eta)}{\mathrm{P} \times \mathrm{A} \times \Delta\mathrm{P}}} \tag{7}$$

where p is the membrane porosity, ΔP is the applied pressure, l is the thickness, A is the membrane effective area, η is water viscosity (0.00089 Pa.s), and Q is the pure water flux (m^3/s).

Table 3
Different analytical instruments used.

Instrument	Model	Properties Studied
Fourier Transform Infrared Spectroscopy (FT-IR)	Thermo Scientific Nicolet spectrometer	Functional groups, chemical bonding
Field Emission Scanning Electron Microscope (FESEM)	Zeiss EVO LS15 SEM, Zeiss, Sydney, Australia	Surface morphology, microstructure
Energy-dispersive X-ray Spectroscopy (EDAX)	Bruker SDD XFlash 5030 detector, Zeiss, Australia	Elemental composition
Inductively Coupled Plasma Mass Spectrometry (ICP-MS)	Agilent Technologies	Ion concentration
Rotating shear rheometer	Local Manufacturer	Rheological properties, Mechanical strength
Water Contact Angle (WCA) measurement	Kyowa Interface Science, Chennai, India	Wettability, hydrophilicity/ hydrophobicity
Nano-ZS Zeta-sizer	Malvern Analytical	Zeta Potential
TOC Analyzer	Shimatzu, Japan	Total Organic Carbon
X-Ray Diffractometer	Bruker D8 Discover	Crystal structure, phase identification, interlayer spacing

3. Results and discussion

3.1. Physiochemical properties

3.1.1. FTIR

The peaks detected in the FTIR spectrum of κC ranging from 800 to 1200 cm^{-1} correspond to specific polysaccharide units: 3,6-anhydro-galactose and d-galactose-4-sulfate (Fig. 2a). This alignment with previous literature on κC hydrogel analysis indicates these peaks stem from stretching bands of C–O, O═S═O, C–H, and O–H groups, affirming the existence of carboxyl (-COOH), hydroxyl (-OH), and other polar functional groups [24,28].

The introduction of nZVI nanoparticles into κC induces a significant increase in the transmittance of the -OH bond within the 3000–3750 cm^{-1} range. This change signifies that nZVI nanoparticles alter hydrogen bonding interactions within the κC matrix, resulting in a broader peak within this spectral range [29,30]. Additionally, spectral changes are evident in the 800–1200 cm^{-1} region, where peaks related to C-O and C-H bonds display broadening. At the peak near 1640 cm^{-1} , due to carbonyl (C═O) stretching vibrations indicative of ester linkages within κC, a reduction in sharpness is observed [31–33].

Incorporating PEI alongside nZVI further influences the FTIR spectrum of κC. Despite the addition of a small amount of PEI, its primary impact lies in enhancing the interaction potential with κC's functional groups, including -COOH and -OH. PEI's amine groups likely contribute to additional peaks in the spectrum, especially around 1590 cm^{-1} , associated with N-H bending vibrations of secondary amines [34]. These observations underscore the interactions facilitated by both PEI and nZVI nanoparticles within the κC matrix, impacting its structural integrity and functional properties [27].

The FTIR analysis reveals significant interactions between the components of the composite hydrogel membrane. As shown in Fig. 2b, both electrostatic forces and hydrogen bonding are involved: PEI's amine groups form hydrogen bonds with the hydroxyl groups of κC, while electrostatic interactions occur between PEI and the sulfate groups in κC. nZVI, on the other hand, interacts primarily through electrostatic attraction with the anionic sulfate groups of κC. These combined interactions strengthen the matrix and modify the functional group environment, as reflected in the observed spectral changes.

FTIR spectra analysis was performed on κC-ZVI2 * to provide deeper insight into the rejection mechanisms, as illustrated in Fig. 2c. The broadening in the 3000–3600 cm^{-1} region is a sign of enhanced hydrogen bonding, as hydroxyl (O-H) and amino (N-H) groups form extensive networks with water molecules and contaminants, reflecting the hydrogel's increased hydration and interaction with wastewater components. Similarly, the broadening between 900 and 1200 cm^{-1} points to complex interactions involving the C-O and S-O stretching vibrations in the hydrogel's polysaccharide backbone. The result suggests the binding of heavy metals to sulfonate groups and other structural adjustments within the hydrogel, such as changes in cross-linking density and conformational adaptations [35,36].

The new peaks at 438 and 474 cm^{-1} signify the formation of metal-oxygen (M-O) bonds, reflecting the hydrogel's ability to bind heavy metals effectively. Specifically, the nZVI component can undergo partial oxidation during the treatment, forming iron oxides or hydroxides, which exhibit characteristic Fe-O stretching vibrations within this range. These new iron oxide formations suggest that the nZVI is actively participating in capturing contaminants, transforming them into compounds that facilitate strong metal binding. Concurrently, the shift to higher wavenumbers from 441 to 449 $cm^{-1}$and from 518 to 524 cm^{-1} indicates that these M-O or Fe-O bonds have become stronger and shorter, signaling enhanced bond strength and tighter integration of metal ions into the hydrogel matrix. This increased bond strength could

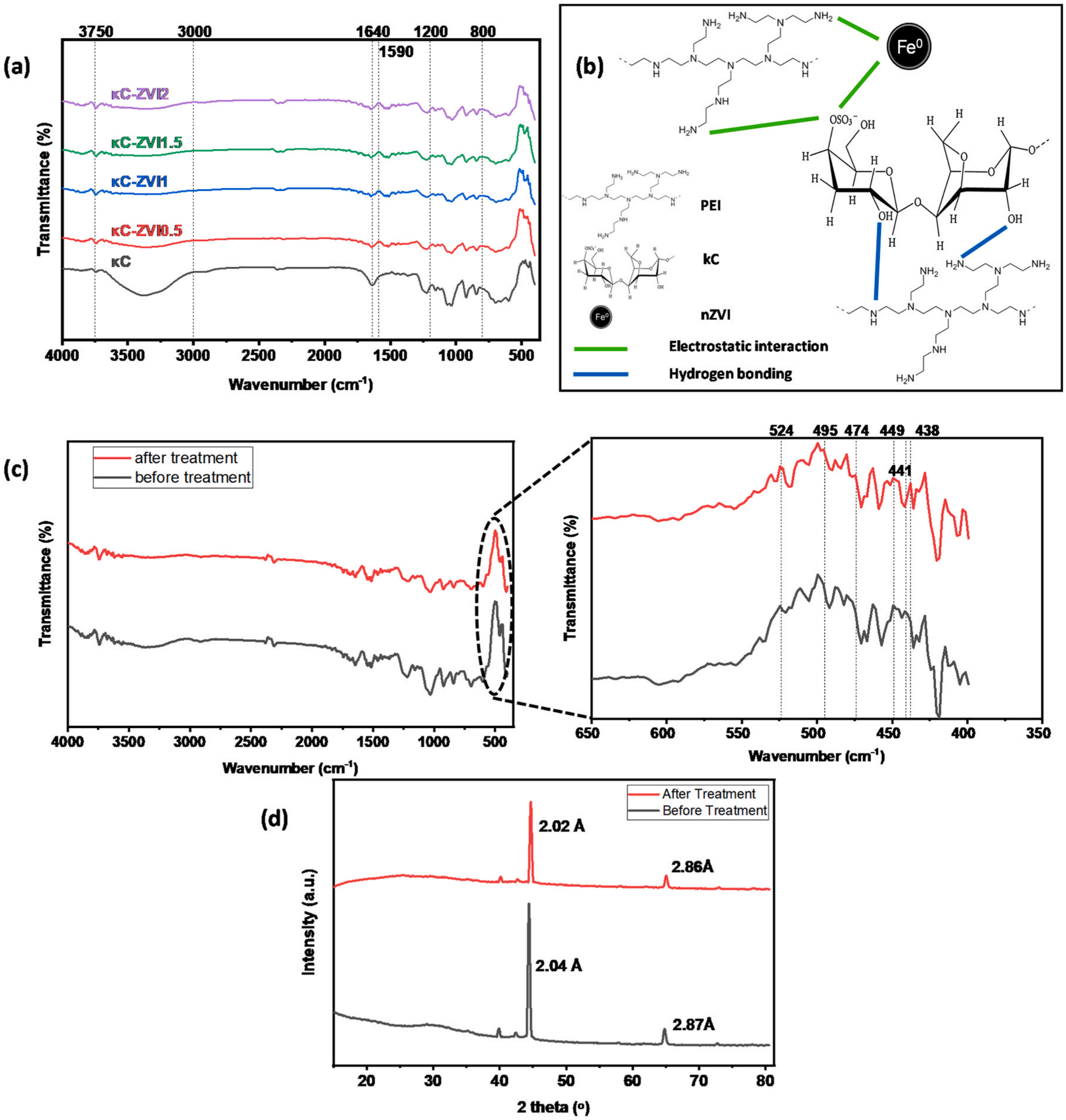

Fig. 2. (a) FT-IR spectra of the κC and κC loaded with nZVI, (b) Molecular interactions within in kC-ZVI hydrogel, (c) FTIR spectra of κC-ZVI2 * before and after treatment with wastewater, (d) XRD analysis of κC-ZVI2 * before and after treatment with wastewater.

result from the oxidation of nZVI and subsequent interaction with heavy metals, leading to a more rigid and stable structural environment [37–40].

3.1.2. XRD

X-ray diffraction (XRD) analysis was performed on the optimum membrane, kC-ZVI2 * , before and after treatment with landfill leachate wastewater. The broad peak observed around 20° to 30° (Fig. 2d) in the XRD pattern is characteristic of the amorphous structure of kappa-carrageenan (kC), consistent with its disordered polymer network [41]. The XRD patterns revealed two major peaks corresponding to Fe° at approximately $2\theta = 45^\circ$ and 65° in both the pristine and treated membranes [42]. After treatment, the first peak at 45.33° shifted slightly to 45.73°, indicating a change in the crystalline structure of the nZVI. This shift is likely due to the oxidation of Fe° or chemical interactions with contaminants in the wastewater, which can modify the lattice structure. Additionally, the decrease in peak intensity post-treatment suggests a reduction in crystallinity, possibly due to the transformation of Fe° into less crystalline iron oxides [43,44].

The slight decrease in d-spacing (from 2.04 Å to 2.02 Å for the first peak and from 2.87 Å to 2.86 Å for the second peak) further supports minor structural modifications in the membrane after treatment. These changes may result from the oxidation of nZVI or interactions with contaminants, leading to slight compaction of the membrane structure.

3.1.3. Water uptake, swelling, water contact angle

To assess water uptake (WU), fresh hydrogel samples were compared with dried samples. The composite hydrogels, each with a thickness of 1 cm, were utilized for the WU analysis. The hydrogel shrunk and turned into a small plastic-like structure upon exposure to heat. Analysis of the WU reveals that hydrogel water uptake decreases with nZVI loading, as depicted in Fig. 3a. Remarkably, the WU of κC-ZVI0.5 demonstrates a capacity for absorbing up to 925 g of water per gram. The observed decrease in water uptake suggests that nZVI nanoparticles promote cross-linking within the κC matrix, leading to tighter network structures. This increased cross-linking reduces the availability of free water

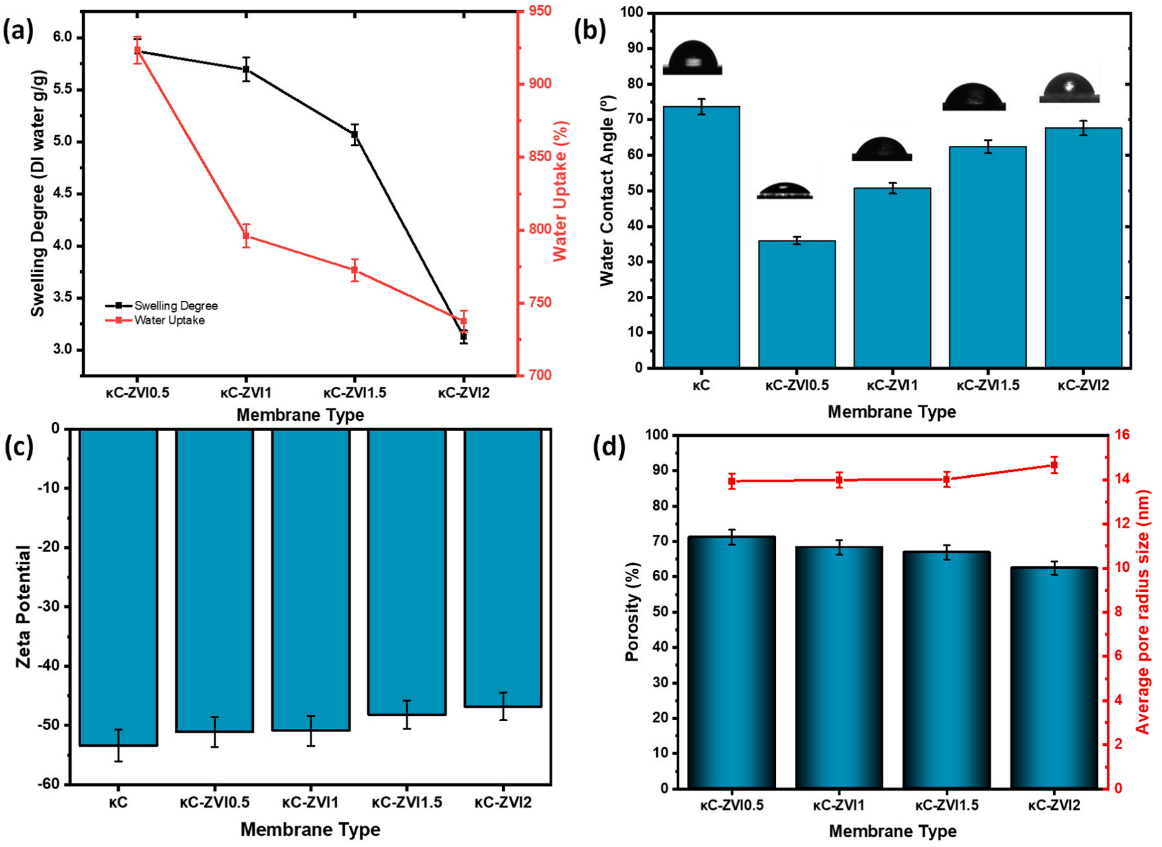

Fig. 3. (a) Swelling degree in DI water and Water uptake of composite hydrogels with different nZVI concentrations, (b) Contact angle measurements of pure κC and composite hydrogels with different nZVI concentrations, (c) Zeta potential measurements for the composite hydrogels with different nZVI concentrations, (d) the effects of nZVI concentration on the porosity and average pore size.

molecules to interact with the polymer chains, thereby decreasing water uptake [45,46].

The swelling behaviour of hydrogels with different proportions of nZVI was examined by immersing the hydrogels in DI water for 2 hours. The ability of the hydrogel to swell increases in direct proportion to its porosity. Factors such as the network formulation, carrageenan polymer chains, and cross-linking density significantly influence pore size, pore volume fraction, and interconnectivity. The effect of varied concentrations on swelling is depicted in Fig. 3a. The incorporation of nZVI nanoparticles leads to increased cross-linking or reduced availability of free water molecules within the κC matrix, resulting in a decrease in the swelling degree due to the tighter network structure or reduced water accessibility would hinder the polymer chains' ability to swell and absorb water. In other words, a higher concentration of nZVI nanoparticles in the films leads to increased hydrogen bonds between nZVI and the κC matrix. Consequently, the affinity of free water molecules towards the nanocomposite hydrogels decreases by nZVI loading [45–47].

The water contact angle exhibits a distinct trend with varying nZVI concentrations (Fig. 3b). Initially, as the nZVI concentration increases to 0.5 %, the water contact angle dramatically decreases from 73.66° to 36°. This significant reduction indicates enhanced hydrophilicity and wettability of the surface, likely due to the introduction of nZVI particles, which can increase surface roughness and introduce hydrophilic sites [48]. However, the water contact angle increases as the nZVI concentration increases from 0.5 % to 2. Although this rise suggests a slight reduction in surface hydrophilicity, the contact angle remains lower than that of pure κC. This pattern could be attributed to the saturation effect of nZVI particles on the surface properties. At higher concentrations, the excess nZVI may lead to particle agglomeration or a change in surface morphology, reducing the available surface area for water interaction and slightly disrupting the hydrophilic nature of the hydrogel [49].

Despite this increase, the κC with higher nZVI concentrations still exhibits better wettability than the pure κC. The surface zeta potential of κC and its composites with nZVI was measured, and the results are presented in Fig. 3c. The zeta potential values for κC and κC with 0.5 %, 1 %, 1.5 %, and 2 % nZVI loadings were recorded as −53.4 mV, −51.1 mV, −50.9 mV, −48.2 mV, and −46.8 mV, respectively. The increasing nZVI concentration led to a gradual decrease in the magnitude of the negative zeta potential due to the presence of nZVI particles, which reduce the surface charge of the membrane by neutralizing some of the negative charges associated with kappa carrageenan's carboxyl and sulfate groups [50]. Additionally, the inclusion of a 1 % wt./v of PEI, a polycation, further contributed to the reduction in negative charge by introducing positively charged amine groups [51]. These changes in surface charge could enhance the selectivity and rejection performance of the membrane, as the reduction in negative zeta potential modifies the electrostatic interactions with ions in the feed solution. The results are consistent with previous findings, where the introduction of additives like ZVI and PEI influenced the surface charge and membrane performance [52,53].

3.2. Morphology and elemental analysis

3.2.1. Porosity and pore size

Fig. 3d depicts the impact of nZVI concentration on the porosity and pore size of kC hydrogel membranes. As nZVI concentration increased from 0.5 % to 2 %, membrane porosity decreased from 71.3 % for kC-ZVI0.5 to 68.3 %, 67.0 %, and 62.5 % for kC-ZVI1, kC-ZVI1.5, and kC-ZVI2, respectively. This reduction is due to increased cross-linking and physical filling. Indeed, nZVI enhances the hydrogel's network density, restricting solvent mobility and occupying internal voids, resulting in a more compact structure with fewer interconnected pores.

With nZVI concentration increase, the void morphology of the membranes gradually changes, leading to a more compact structure. According to Eq. (7) and Fig. 3d, the pore radius for the kC-ZVI0.5 membrane was 13.93 nm, which slightly increased to 13.98, 14.01, and 14.66 nm with nZVI addition. The slight increase in pore size can be attributed to the interaction of nZVI particles with the kC matrix, creating localized expansions that result in larger average pore sizes. Additionally, nZVI can block smaller voids, leaving larger pores relatively unaffected. These combined effects contribute to the observed changes in pore structure within the hydrogel.

3.2.2. FESEM and EDX

The surface morphology of both the pristine κC membrane and the membranes containing 2 % nZVI (κC-ZVI2 *) are depicted in the SEM images. These images illustrate the morphological changes induced by the nZVI introduction. The SEM images reveal an absence of cracks. The pure κC membrane features a smooth surface, as shown in Fig. 4. In contrast, the κC-ZVI2 * membrane reveals significant physical alterations, including visible wrinkle formations. Embedding nZVI particles into the hydrogel can create surface irregularities, resulting in a rougher membrane surface. This increased roughness offers more potential sites for adsorbing contaminants from the feed solution. nZVI particles are uniformly distributed across the hydrogel surface, preserving the hydrogel's overall structural integrity [21,54].

The cross-sectional SEM images reveal distinct morphological differences between the κC and κC-ZVI2 * membranes. The κC membrane exhibits a relatively smooth and dense structure with a well-defined layered arrangement. In contrast, the κC-ZVI2 * membrane presents a rougher and more porous morphology, indicating the influence of nZVI incorporation on membrane structure. These structural variations highlight the impact of nZVI on membrane formation, which may contribute to improved separation performance in water treatment applications.

The elemental analysis of the nanocomposite hydrogel is presented in Table 4. After testing with $MgSO_4$, NaCl, and landfill leachate wastewater, the EDAX results reveal compositional changes. Following exposure to $MgSO_4$, magnesium (Mg) appears in the hydrogel, indicating Mg^{2+} incorporation, along with increased sulfur (S) levels due to additional sulfate ions (SO_4^{2-}). Exposure to NaCl introduces sodium (Na), showing Na^+ uptake by the hydrogel. Across all tests, including landfill leachate wastewater, the iron (Fe) content decreases, likely due to membrane fouling. In addition, heavy metals and ions in the feed may compete for binding sites or chemically alter Fe, reducing its detectable content. The leachate also introduces heavy metals into the hydrogel, demonstrating its capacity for contaminant capture.

3.3. Mechanical properties

The rheological properties of pure κC and κC loaded with 0.5–2 % nZVI (Fig. 5) exhibit non-Newtonian shear-thinning behavior, consistent with the Herschel-Bulkley model. Pure κC forms a gel that shows a decrease in viscosity as the shear rate increases, indicating its shear-thinning nature. This behavior is characterized by a yield stress, beyond which the gel begins to flow, and a flow behavior index (n) less than 1, typical of shear-thinning fluids. The viscosity and yield stress of κC increased with increasing nZVI loading in the hydrogel membrane. At lower nZVI concentrations (0.5 %), the viscosity and yield stress increase is less pronounced while, at higher concentrations (1–2 %), these properties increase significantly, suggesting that nZVI particles reinforce the gel network. Despite the overall higher viscosity, the κC-ZVI composites still exhibit viscosity reduction with increasing shear rate, maintaining the non-Newtonian shear-thinning behavior and aligning with the Herschel-Bulkley model parameters [55,56].

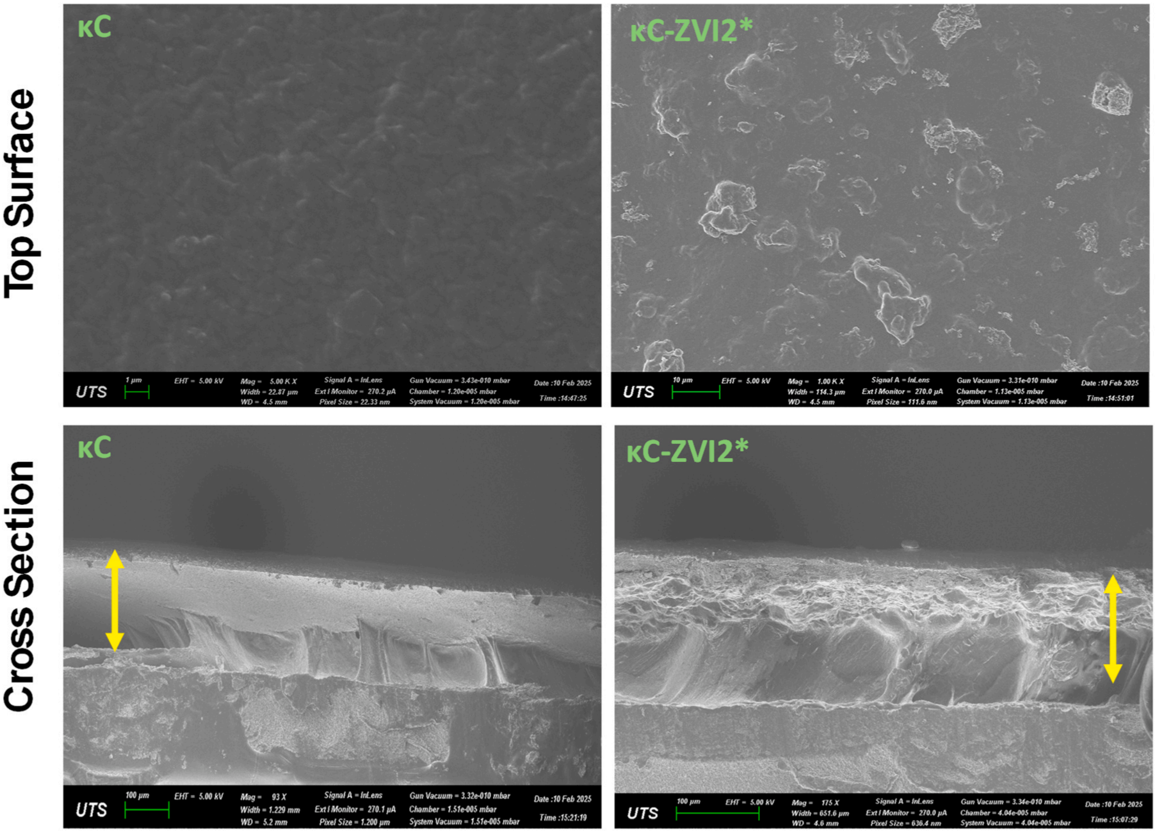

Fig. 4. SEM analysis of the pure κC membrane and κC-ZVI2 * .

Table 4
Composition of the element of κC-ZVI2 * before and after treatment analyzed by the EDX.

Sample	Elemental Composition wt%												
	C	O	Fe	S	K	Al	Na	Mg	Co	Cu	Ca	Mn	Ni
κC-ZVI2 * before treatment	20.65	35.22	24.99	4.99	4.65	-	-	-	-	-	1.63	-	-
κC-ZVI2 * after Na treatment	21.74	45.81	16.95	5.01	3.87	-	0.89	-	-	-	2.05	-	-
κC-ZVI2 * after Mg treatment	24.23	48.43	12.01	6.96	3.98	-	-	0.93	-	-	1.89	-	-
κC-ZVI2 * after wastewater treatment	24.66	49.95	7.01	6.00	3.03	0.18	0.69	0.27	0.09	0.01	2.02	0.07	0.08

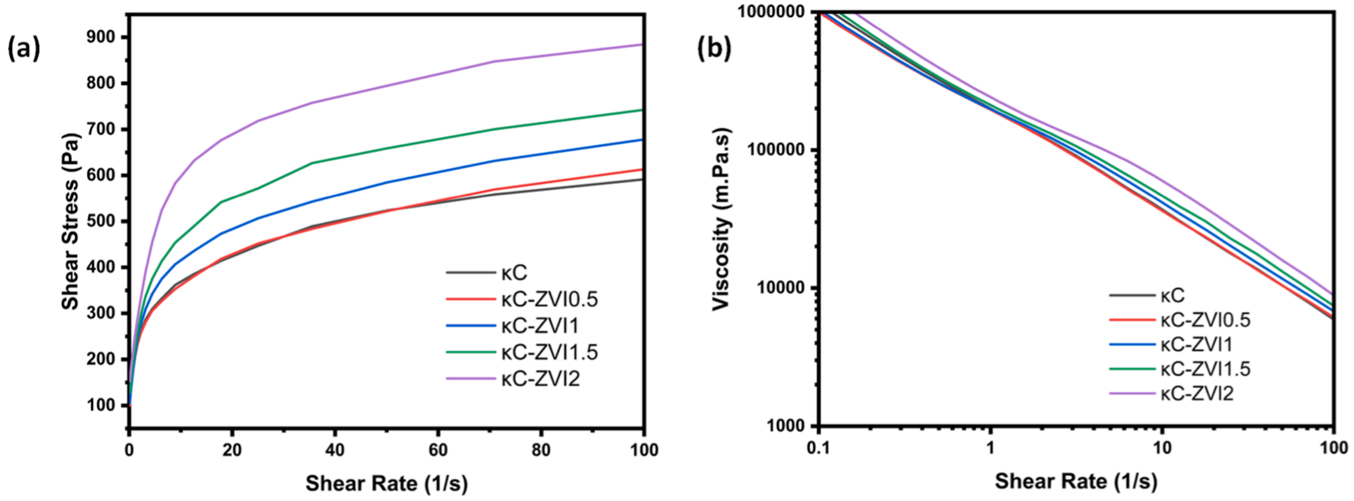

Fig. 5. Mechanical strength of Hydrogel with various nZVI loading at room temperature: (a) stress rate versus shear rate, and (b) viscosity versus shear rate.

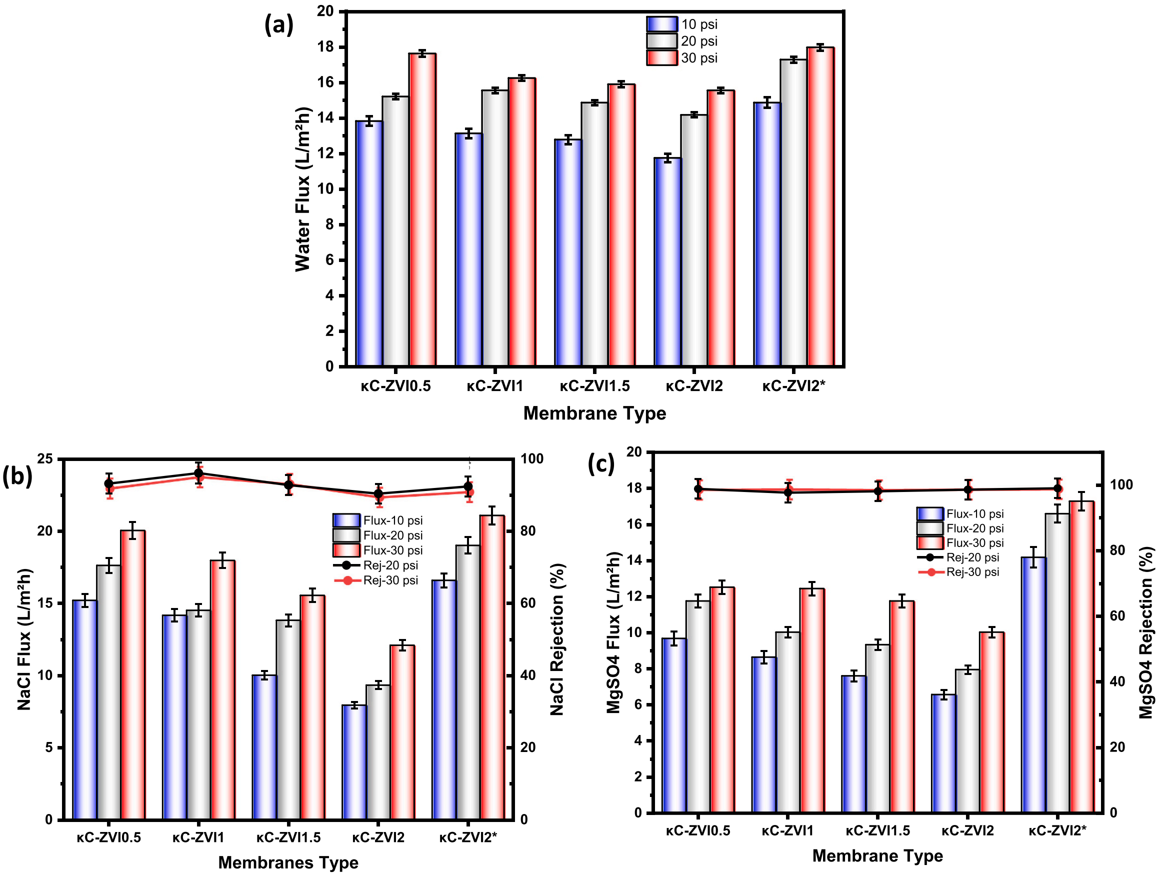

Fig. 6. (a) Pure water flux with DI water, (b) NaCl flux (2 g/L) and rejection, (c) $MgSO_4$ flux (2 g/L) and rejection for different membranes.

3.4. Water flux and rejection

The experimental investigation aimed to assess water flux at 10, 20, and 30 psi. Pure water flux in the membrane increased as feed pressure increased from 10 psi to 30 psi due to reducing membrane resistance (Fig. 6a). For example, water flux in the κC-ZVI0.5 membrane increased by 27.5 % from 13.83 L/m^{2}h (LMH) to 17.64 psi when the pressure raised from 10 psi to 30 psi. Fig. 6a also shows that water flux decreased slightly with increasing the nZVI loading from 0.5–2 % due to clogging the hydrogel pores, hindering water flow. At 30 psi pressure, for example, water flux decreased from 16.25 L/m^{2}h in κC-ZVI1 to 15.9 L/m^{2}h in κC-ZVI1.5 because of the higher nZVI loading in the latter membrane. In other words, the presence of nZVI nanoparticles within the membrane matrix introduces additional hydraulic resistance due to increased tortuosity and membrane pores clogging [78,93]. The high water flux in κC-ZVI2 * is due to the lower membrane resistance caused by reducing its thickness from 0.5 to 0.25 cm.

The membranes were tested using 2 g/L NaCl and $MgSO_4$ solutions to assess their permeability and ability to reject NaCl and $MgSO_4$. Both solutions exhibited a similar pattern to pure water flux studies, with reduced water flux as nZVI loading increased due to obstruction of the hydrogel pores diameter and increased membrane tortuosity (Figs. 6b and 5c). This decline in water flux is also due to the increment in transfer resistance caused by the accumulation or adsorption of salt molecules on the membrane surface [21]. With NaCl feed solution, for example, κC-ZVI0.5 achieved a water flux of 15.22 L/m^{2}h at 10 psi, while it dropped to 7.95 L/m^{2}h in κC-ZVI2, reflecting a reduction of approximately 48 %. In contrast, water flux in the κC-ZVI2 * membrane of 0.25 cm thickness reached 16.60 L/m^{2}h at 10 psi, approximately 109 % higher than κC-ZVI2. As the membrane thickness decreased to 0.25 cm, water flux increased due to the lower membrane resistance. As pressure increased to 20 psi, the water flux rose significantly, with κC-ZVI0.5 reaching 17.63 L/m2h, κC-ZVI2 at 9.33 L/m2h, and κC-ZVI2 * achieving 19.02 L/m2h. At 30 psi, the water flux trend continued, with κC-ZVI0.5 reaching 20.06 L/m2h, κC-ZVI2 at 12.10 L/m2h, and κC-ZVI2 * at 21.10 L/m2h. Similar to the behavior observed with NaCl, the $MgSO_4$ water flux exhibited a decreasing trend with increasing nZVI loading (Fig. 6c). For κC-ZVI0.5, the flux reached 9.68 L/m^{2}h at 10 psi, while κC-ZVI2 dropped to 6.57 L/m2h, reflecting a reduction of approximately 32 %. In contrast, the halved-thickness κC-ZVI2 * membrane demonstrated a significant increase in performance, achieving a flux of 14.18 L/m^{2}h at 10 psi, approximately 116 % higher than κC-ZVI2. The highest water flux was 17.29 L/m2h, achieved by the κC-ZVI2 * membrane at 30 psi.

The differences in water flux rates observed among water, NaCl, and $MgSO_4$ solutions can be attributed to several factors. One key factor is the molecular size and structure of the ions. At 30 psi and κC-ZVI2 * membrane, NaCl showed a maximum water flux of 21.10 L/m2h, while $MgSO_4$ reached only 17.29 L/m^{2}h at the same pressure, indicating that Mg^{2+} ions are approximately 40 % less permeable than Na^+ ions. In effect, Mg^{2+} ions have a higher charge density than Na^+ ions, resulting in stronger electrostatic interactions with the hydrogel membrane. The strong interaction causes increased membrane swelling and reduced pore size, limiting water passage. Besides, the negatively charged SO_4 ions are larger and more strongly hydrated than Cl^- ions, further impeding water flux by increasing osmotic pressure and reducing water mobility through the membrane. These combined effects reduce the overall water permeability of the $MgSO_4$ feed solution.

Fig. 6b and c illustrate the rejection performance of the membranes. At 20 psi and NaCl feed solution, the average rejection for the hydrogel membranes was approximately 92.43 %. At 30 psi, rejection rates varied slightly, recording an average rejection of 90.96 %. This consistent rejection efficiency suggests that the hydrogel membranes effectively impede the transport of NaCl ions. The rejection rates of $MgSO_4$ at varying pressures demonstrate exceptional performance by the hydrogel membranes in selectively excluding larger ions. The average rejection rates for $MgSO_4$ by the hydrogel membranes was slightly > 98 % at 20 psi and 30 psi. Compared to the NaCl solution, the significantly higher rejection rates for $MgSO_4$ suggest that the membranes are particularly effective at impeding the transport of divalent Mg^{2+} ions due to their larger hydrated radius compared to Na^+ ions and stronger electrostatic interaction with the hydrogel membrane because of the higher valency of Mg^{2+} and SO_4^{2-} ions.

The remarkable rejection performance of $MgSO_4$ and NaCl observed across all hydrogel samples can be attributed to several factors. Firstly, the hydrogel's porous structure and intricate network of polymer chains act as a physical barrier, effectively sieving out ions based on their size. The pore size hinders larger ions, such as $Mg^{2+,}$ and are thus retained within the hydrogel matrix. Additionally, the hydrogel's charged functional groups and the presence of nZVI nanoparticles contribute to electrostatic interactions with ions, further enhancing their retention. The high degree of cross-linking within the hydrogel matrix ensures stability and prevents ions from permeating through gaps or defects in the structure. Also, each membrane demonstrated a higher rejection rate for $MgSO_4$ compared to NaCl due to the sulfate anion's larger ionic radius (2.42 Å) compared to that of NaCl (1.81 Å) [21,24]. Among the tested samples, κC-ZVI2 * exhibited the highest flux while maintaining excellent rejection rates of 98.83 % and 90.96 % for $MgSO_4$ and NaCl solutions, respectively, at 30 psi, indicating its optimal performance as a filtration membrane for $MgSO_4$ and NaCl solutions. Therefore, κC-ZVI2 * stands out as the preferred choice for applications requiring efficient removal of these ions from aqueous solutions.

3.4.1. Wastewater treatment

To further investigate the performance of the optimal membrane (κC-ZVI2 *), landfill leachate water was utilized as the feed solution without pretreatment. As pressure increases, the driving force for water molecules passage across the membrane also increases, leading to higher water flux. The initial feed concentration percentages are detailed in Table 1. Because of the varying sizes of particles and the intricate composition of landfill leachate, the water flux was less than that of pure water (Fig. 7a) [57]. Particularly noteworthy is the performance of the κC-ZVI2 * membrane, which exhibited remarkable ion rejection rates alongside a water flux of 11 L/m^{2}h at 30 psi.

Three filtration cycles were conducted for wastewater treatment, revealing an increased water flux with the applied pressure. In the first cycle, water flux was 4.84 L/m^{2}h at 10 psi, 6.22 L/m^{2}h at 20 psi, and 11 L/m^{2}h at 30 psi, indicating an increase of approximately 28.5 % from 10 psi to 20 psi and a substantial 72.2 % increase from 20 psi to 30 psi. However, a noticeable decline in water flux was observed in subsequent filtration cycles, particularly at lower pressures. In the second cycle, water flux dropped to 2.42 L/m^{2}h at 10 psi, representing a 50 % reduction compared to the first cycle, while the flux at 20 psi and 30 psi decreased to 5.18 L/m^{2}h and 10.02 L/m2h, respectively, reflecting reductions of 16.7 % and 6.5 %. By the third cycle, the flux further declined to 1.21 L/m^{2}h at 10 psi, 3.11 L/m^{2}h at 20 psi, and 7.26 L/m^{2}h at 30 psi, showing a 50 % decrease at 10 psi compared to the second cycle and an almost 40 % drop at 20 psi. This reduction can be attributed to the membrane fouling and pore-clogging caused by organic and colloidal particles (Table 1) over multiple filtration cycles. Also, the greater water flux decline at 10 psi is probably due to the longer filtration time to process the same feed volume for 20 psi and 30 psi, leading to systematic accumulation of the fouling materials on the membrane surface.

As shown in Fig. 7b, the study assessed the removal of Total Organic Carbon (TOC) from leachate wastewater, with a feed TOC concentration of 165.68 mg/L at 20 psi and 30 psi over three filtration cycles. At 20 psi, the κC-ZVI2 * achieved a TOC rejection of 61.05 % in the first cycle, which slightly decreased to 55.8 % and 55.4 % in the second and third cycles, respectively. At 30 psi, the membrane rejected 58.6 % of TOC, followed by 57.4 % in the second cycle and 53.7 % in the third cycle. These results demonstrate a gradual decline in TOC rejection over

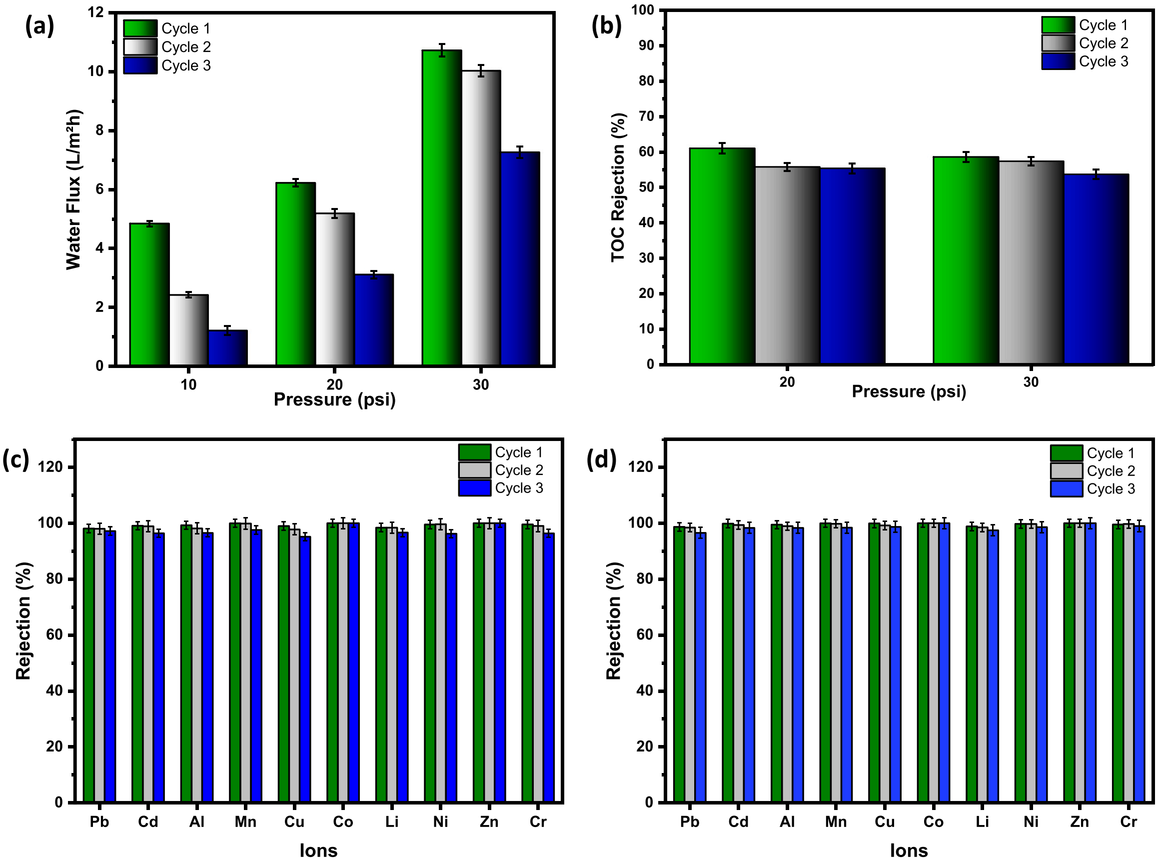

Fig. 7. (a) Water flux for landfill leachate wastewater, (b) TOC Rejection, (c) Rejection of heavy metal ions from the landfill leachate wastewater at 20 psi, (d) Rejection of heavy metal ions from the landfill leachate wastewater at 30 psi.

multiple cycles, reflecting the typical decrease in performance observed in membrane systems due to fouling yet maintaining relatively high removal efficiency.

The heavy metals rejection by the κC-ZVI2 * membrane was also studied through three consecutive filtration cycles. Notably, the membranes maintained a high rejection rate over three consecutive cycles, as illustrated in Fig. 7c and d. Two feed pressures, i.e., 20 psi and 30 psi, were investigated, and DI water was filtered through the membrane following each filtration cycle. The κC-ZVI2 * membrane achieved outstanding rejection of metal ions; for example, at 30 psi, the highest rejection rates were recorded for cobalt (Co) and chromium (Cr), with nearly complete removal at 100 % and 99.53 %, respectively. Other heavy metals, including cadmium (Cd), lead (Pb), aluminum (Al), lithium (Li), and nickel (Ni), also exhibited excellent rejection rates exceeding 98 %, with 98.69 % for Pb, 99.83 % for Cd, 99.46 % for Al, 99.97 % for Mn, 99.92 % for copper (Cu), 99.74 % for Ni, and 100 % for Zn.

Several mechanisms contribute to the rejection of metal ions by the hydrogel, including adsorption, ion exchange, and chelation. kC, as an ionic polysaccharide, is highly sensitive to charged species in solution, which can alter its conformation from ordered to disordered. It interacts with metal ions by forming bridges with their d-galactose sulfate groups and electrostatically interacting with other d-galactose rings. It exhibits a strong affinity for heavy metals like cadmium, lead, and mercury due to the sulfate groups in its molecule, which are capable of forming coordinated covalent bonds with these ions. This chelation process involves the formation of coordination bonds between the sulfate groups and the heavy metal ions, facilitating the removal of heavy metals from the solution as insoluble complexes. Additionally, κC can sequester heavy metals through adsorption, where metal ions physically bind to the surface of the hydrogel without forming coordination bonds. These mechanisms collectively contribute to the efficient removal of heavy metals from solution by κC hydrogels [24,36].

Moreover, the rejection of divalent metal ions by hydrogel membrane is governed by the formation of coordination complexes between the metal ions and the active functional groups (>C═O, -OH, -CONH-) on the kC hydrogel surface. The efficiency of ion rejection is also influenced by the membrane's large surface area and pore size, which facilitate the capture and transport of metal ions. The porous, three-dimensional structure of hydrogel-based membranes enhances their ability to remove contaminants from wastewater. Incorporating magnetite nanoparticles like nZVI into the membrane further increases surface area and pore size, allowing more space for metal ions accumulation and improving overall adsorption performance [58]. Both nZVI and PEI are effective in removing heavy metals through different mechanisms. The nZVI comprises a metallic iron core enveloped by an amorphous oxide shell that functions primarily through reduction and adsorption processes. The metallic iron core exhibits well-defined reducing properties, functioning as an electron donor. Metallic iron demonstrates significant reductive capability in aqueous environments. Its extensive surface area facilitates the rapid release of electrons. Consequently, heavy metals possessing standard reduction potentials considerably higher than that of iron, such as Cu^{2+}, can be rapidly reduced via the following reaction [25,59,60].

$$Fe + Cu^{2+} \rightarrow Fe^{2+} + Cu \tag{1}$$

This mechanism also applies to other heavy metals, where the reduction of lead ions causes their precipitation:

$$Fe + Pb^{2+} \rightarrow Fe^{2+} + Pb(OH)_2\downarrow \tag{2}$$

In this process, lead ions can react with hydroxide ions formed from nZVI corrosion, leading to the precipitation of lead hydroxide and enhancing the overall removal efficiency. Electrostatic attraction and adsorption are also critical in the rejection of heavy metals. The surface properties of nZVI, particularly when oxidized, can develop charges that interact favorably with positively charged heavy metal ions. The corrosion of nZVI in an aqueous environment leads to iron hydroxide formation and other precipitates, providing additional reactive sites for heavy metals to adsorb onto. This co-precipitation process is particularly effective for ions such as Ni^{2+}, Zn^{2+}, and Pb^{2+}, contributing significantly to their removal from solution [25,61,62].

The slight variation in rejection rates among different ions can be explained by considering their ionic and hydrated radii alongside their standard redox potentials. For instance, the rejection of Cr^{3+} exhibited a strong efficiency of 99.53 %. This performance may be attributed to its relatively small ionic radius and hydration characteristics, which facilitate favorable interactions with the hydrogel. Similarly, Co^{2+} achieved a 100 % rejection rate, underscoring the hydrogel's effective binding capacity for this ion [54].

PEI also plays a role in heavy metal removal through complexation and ion exchange mechanisms. Its abundant amine groups form coordinated covalent bonds with heavy metal ions, sequestering them from the solution. Moreover, PEI can undergo ion exchange reactions with heavy metal ions, effectively replacing them with other cations [26,27]. The κC-ZVI2 * membrane's high rejection of most heavy metals presents a great potential for valuable metal ions recovery, such as Li^+, Co^{2+}, Ni^{2+}, and Pb^{2+}, from wastewater for reuse in industries, reducing their environmental impact.

3.4.2. Performance comparison

The performance of κC-ZVI2 * hydrogel membrane was compared to previously reported hydrogel studies, as shown in Table 5. The membranes developed in this study demonstrated superior performance, particularly rejection of metal ions, compared to earlier studies. This improvement is likely due to the synergistic effects of nZVI and PEI cross-linking, enhancing the hydrogel structure. Although previous hydrogel membranes achieved high water flux, they failed to achieve a high rejection rate for a wide range of divalent and monovalent ions. For example, sodium alginate-CNF- biochar membrane achieved 91.4–96.8 % of Cr^{3+} and Cr^{6+} at 3.5 bar, but there is no data about monovalent and divalent ions rejection [57]. In another study, a gravity-driven cellulose acetate (CA) carbon-based aluminum hydroxide (CACG) was employed for the rejection of a wide range of divalent ions, exhibiting > 90 % rejection for most divalent ions but low rejection to monovalent ions [59]. Sodium Alginate- PEG- CNF- MWCNT-COOH membrane was employed for organic and inorganic treatment and showed 85.7–99.8 % rejection of multiple dyes but low rejection of metal ions, circa 10 % [65]. In contrast, the κC-ZVI2 * membrane in this study achieved outstanding rejection of monovalent ions, > 90 %, and divalent ions, > 98 %, at 2.06 bar feed pressure. The membrane also showed a constant rejection rate of these ions over multiple filtration cycles, indicating a steady membrane performance. The membrane demonstrated a decent water flux of 11 L/m^2h at 2.06 bar but decreased in the consecutive filtration cycles since the leachate wastewater had not been pretreated.

Compared to previous studies (Table 5), the κC-ZVI membrane exhibited a higher rejection rate of heavy metals due to its outstanding permselectivity characteristics, which is a trade-off between the membrane permeability and selectivity. Higher membrane selectivity refers to its tight molecular structure that would be achieved at the expense of the membrane permeability. For example, this study achieved 99 % rejection of heavy metals and 18 L/m^2h water flux compared to 61.5 L/m^2h in [63] but a lower rejection rate of heavy metals. Studies [54] and [24] achieved higher water flux than in this study but lower rejection rates of heavy metals. In studies [64] and [69], more permeable membranes were used for large molecular weight dye rejection from wastewater. Therefore, κC-ZVI membrane performance is desirable when high rejection is crucial for wastewater treatment and metals recovery.

4. Lithium and lead recovery

The recovery of lithium and lead from wastewater is crucial due to their industrial significance and environmental impact. Lithium is a key component in batteries for electric vehicles and renewable energy storage, with growing demand driving efforts to recover it from secondary sources, reducing reliance on mining. Lead is highly toxic and poses severe environmental and health risks, especially in contaminated water supplies. Recovering lead helps prevent pollution and supports recycling in batteries and other industrial applications [72].

The kC-ZVI2 * membrane was evaluated for its ability to recover Lithium and Lead ions from leachate wastewater. The dead-end filtration mode in the kC-ZVI membranes with > 90 % recovery rate assists in heavy ions recovery at the end of the tests by desorption instead of ions recovery from large brine volume on the reverse osmosis and nanofiltration process with much lower recovery rates. The desorption process was carried out by dissolving the membrane in a 0.1 M HCl solution and shaking it at 150 rpm for 24 hours at room temperature. Following this, the solution was centrifuged at 10,000 rpm for a 15-minute to separate the membrane from the metal-enriched solution. Samples from the supernatant were collected and analyzed using ICP-MS to determine the concentrations of various metals.

The recovery rates for lead and lithium were notably high, with lead showing a recovery rate of 68.32 % and lithium at 66.31 %. These results indicate that the κC-ZVI composite membrane is particularly effective in extracting these metals from leachate wastewater. The high recovery percentages highlight the membrane's selectivity and affinity for these ions, suggesting its potential application in the treatment of wastewater containing valuable metals like lead and lithium for their reuse in industries.

5. Conclusion

This study examined the potential of a kappa-carrageenan-zerovalent iron-polyethyleneimine composite hydrogel membrane for wastewater treatment and ion removal. Compared to traditional treatment technologies, this composite hydrogel offers advantages such as cost-effectiveness, environmental friendliness, ease of use, and low energy consumption. The findings reveal several critical insights regarding the efficacy of these composite hydrogel membranes in water treatment.

Notably, while an increase in nano zerovalent iron (nZVI) loading resulted in water flux reduction due to factors like increased hydraulic resistance and cross-linking, the membranes still exhibited high rejection rates for various contaminants, particularly heavy metal ions. The κC-ZVI2 * membrane demonstrated the highest rejection rates (over 98 %) for metals such as Pb, Ba, Al, Cr, and Cd while maintaining a relatively high water flux of 11 L/m2h. This indicates that κC-ZVI2 * is well-suited for practical applications in water treatment systems, achieving a favorable balance between water permeability and rejection efficiency.

In conclusion, these findings underscore the potential of composite hydrogel membranes as effective materials for water purification, offering promising solutions to water quality challenges. Future research should focus on enhancing long-term stability through diverse additives incorporation into the κC during fabrication. Additionally, ongoing studies will aim to optimize operational parameters and tailor the hydrogel for various wastewater treatment applications. Investigating strategies to mitigate fouling and exploring the hydrogel's capacity for resource recovery from waste streams will also be crucial for advancing its practical implementation.

Environmental statement

Leachate contains decent concentrations of valuable metal ions, including lithium, cobalt, nickel, and lead. While these metals are a risk to living beings if they reach the environment, they comprise a valuable

Table 5
Comparison of the performance of κC-ZVI membranes with studies reported in the literature.

Type of hydrogel membrane	Feed	Feed Concentration (mg/L)	Pure Water Flux (L/m^{2}h)	Pressure (bar)	Rejection (%)	Reference
Sodium Alginate-CNF- biochar	Cr^{3+}	200	61.5	3.5	96.8	[63]
	Cr^{6+}				91.4	
carbon-based aluminium hydroxide polyhydrate	Pb	10	123.8	0.015	99.9	[54]
	Cu				99.9	
	Ca				84	
	Mg				85	
	Ba	1			> 90	
	Mn	0.1				
	Ni	3.27				
	Zn	4.4				
	Pb	6.63				
	As	5.69				
	Cu	6.27				
PES- chitosan-aminopropyl silane graphene oxide	BSA	200	123.8	3	98	[64]
	Pb	50			82	
	CI Reactive Blue 50	100			90.5	
	CI Reactive Green 19	100			98.5	
cellulose acetate (CA) carbon-based aluminium hydroxide (CACG)	Pb	1000	30	0.015 (Gravity)	97.4	[65]
	Cu				95	
	Ca				29.5	
	Mg				84.5	
	Mn	0.1			93	
	Ni	3.27			99.6	
	Zn	4.4			96	
	Pb	6.63			98.3	
	As	5.69			99.9	
	Cu	6.27			96	
sodium alginate (SA)-cellulose nanofiber (CNF)	Pb	50	71.5	3.5	100	[66]
	Cu				94.6	
	Cd				88.6	
PES- Chitosan (CTS) and 1,3,5-triglycidyl isocyanurate (TGIC)	Mg	500	47.88	6	94.2	[67]
calcium alginate-polyacrylamide	BSA	500	25	1	98.53	[68]
	Brilliant Blue G250	100			99.64	
kappa-Carrageenan-vanillin	Na	2000	85	0.29 (Gravity)	42	[24]
	Cu				78	
	Mg				72	
	Al	0.06			80	
	Ba	0.42			88	
	Pb	0.007			79	
	Cd	0.008			72	
	Mn	0.07			83	
Ba^{2+}/ Ca^{2+}/-Sodium Alginate	Methyl blue	60	43.5	1	99.6	[69]
	Na	1000			8.2	
Ca^{2+}/-Sodium Alginate- PAAm- PEG-POSS	Methyl blue	500	11.7	2	93	[70]
	Congo red				95	
Sodium Alginate- PEG- CNF- MWCNT-COOH	Crystal Violet	100	51.6	1	99.8	[71]
	Congo red				98.9	
	Tartrazine				93.1	
	Methyl blue				85.7	
	$MgSO_4$	500			11.6	
	Na_2SO_4				10.5	
	$MgCl_2$				9.1	
	NaCl				7.3	
kappa-Carrageenan-nano Zero Valent Iron- PEI	NaCl	2000	18	2.06	90.96	This Work
	$MgSO_4$				98.83	
	Cd	1.64			99.82	
	Pb	1.71			98.68	
	Al	1.78			99.46	
	Cr	1.78			99.53	
	Mn	1.83			99.96	
	Li	2.07			98.85	
	Co	1.72			100	
	Ni	1.68			99.72	
	Cu	1.76			99.91	
	Zn	1.84			100	

source of precious ions. This investigation fabricated and tested a kappa carrageenan (kC) membrane crosslinked with polyethylenimine (PEI) and decorated with nZVI to advance its rejection and minimize swelling. The membrane achieved 98 % rejection of divalent ions, including lithium and lead, and 90 % rejection of NaCl at 30 psi. At the end of the test, 68.32 % and 66.31 % of lead and lithium ions were recovered from the wastewater.

CRediT authorship contribution statement

Altaee Ali: Writing – original draft, Validation, Supervision, Resources, Methodology, Investigation, Data curation, Conceptualization. **Alsaka Lilyan:** Writing – original draft, Validation, Formal analysis, Data curation. **Kardani Rokhsare:** Writing – original draft, Validation, Investigation, Formal analysis, Data curation, Conceptualization. **Yadav Sudesh:** Writing – original draft, Visualization, Validation, Investigation, Formal analysis, Data curation. **Zhou John:** Writing – original draft, Supervision, Methodology, Investigation, Formal analysis.

Declaration of Competing Interest

The authors declare that they have no known competing financial interests or personal relationships that could have appeared to influence the work reported in this paper.

Data availability

Data will be made available on request.

References

[1] Trishitman, D., et al., 2020. Reverse osmosis for industrial wastewater treatment. Curr Trends Future Dev (Bio-) Membr 207–228.

[2] Jun, B.-M., et al., 2020. Applications of metal-organic framework based membranes in water purification: a review. Sep Purif Technol 247.

[3] Mancosu, N., et al., 2015. Water scarcity and future challenges for food production. Water 7 (12), 975–992.

[4] Kolluru, S.S., et al., 2021. Heavy metal removal from wastewater using nanomaterials-process and engineering aspects. Process Saf Environ Prot 150, 323–355.

[5] Xiang, H., et al., 2022. Recent advances in membrane filtration for heavy metal removal from wastewater: a mini review. J Water Process Eng 49.

[6] Shrestha, R., et al., 2021. Technological trends in heavy metals removal from industrial wastewater: a review. J Environ Chem Eng 9 (4).

[7] Hailemariam, R.H., et al., 2020. Reverse osmosis membrane fabrication and modification technologies and future trends: a review. Adv Colloid Interface Sci 276, 102100.

[8] Yang, Z., et al., 2019. A review on reverse osmosis and nanofiltration membranes for water purification. Polymers 11 (8).

[9] Kardani, R., et al., 2018. Effects of nanofillers on the characteristics and performance of PEBA-based mixed matrix membranes. Rev Chem Eng 34 (6), 797–836.

[10] Ismail, N.H., et al., 2020. Hydrophilic polymer-based membrane for oily wastewater treatment: a review. Sep Purif Technol 233.

[11] Mohammadzadeh Pakdel, P., Peighambardoust, S.J., 2018. A review on acrylic based hydrogels and their applications in wastewater treatment. J Environ Manag 217, 123–143.

[12] Yazdi, M.K., et al., 2020. Hydrogel membranes: a review. Mater Sci Eng C Mater Biol Appl 114, 111023.

[13] Mohammadzadeh Pakdel, P., Peighambardoust, S.J., 2018. Review on recent progress in chitosan-based hydrogels for wastewater treatment application. Carbohydr Polym 201, 264–279.

[14] Kabir, S.M.F., et al., 2018. Cellulose-based hydrogel materials: chemistry, properties and their prospective applications. Prog Biomater 7 (3), 153–174.

[15] Pereira, A.G.B., et al., 2021. Recent advances on composite hydrogels designed for the remediation of dye-contaminated water and wastewater: a review. J Clean Prod 284.

[16] Nazzari, E.C., et al., 2022. Hydrogel applications to microbiological water treatment. Sep Purif Rev 52 (3), 155–163.

[17] Chang, H., et al., 2023. State-of-the-art insights on applications of hydrogel membranes in water and wastewater treatment. Sep Purif Technol 308.

[18] Li, W., et al., 2021. Carrageenan-based nano-hybrid materials for the mitigation of hazardous environmental pollutants. Int J Biol Macromol 190, 700–712.

[19] Zia, K.M., et al., 2017. A review on synthesis, properties and applications of natural polymer based carrageenan blends and composites. Int J Biol Macromol 96, 282–301.

[20] Kassab, Z., et al., 2019. Improved mechanical properties of k-carrageenan-based nanocomposite films reinforced with cellulose nanocrystals. Int J Biol Macromol 123, 1248–1256.

[21] Yadav, S., et al., 2022. Surface modification of nanofiltration membrane with kappa-carrageenan/graphene oxide for leachate wastewater treatment. J Membr Sci 659.

[22] Soomro, F., et al., 2023. Highly efficient arginine intercalated graphene oxide composite membranes for water desalination. Langmuir 39 (50), 18447–18457.

[23] Shaikh, Q.-u-a, et al., 2024. Silk fibroin-graphene oxide composite membranes for selective separation of ions and molecules from water. Process Saf Environ Prot 189, 1285–1292.

[24] Ibrar, I., et al., 2023. Kappa carrageenan-vanillin composite hydrogel for landfill leachate wastewater treatment. Desalination 565.

[25] Li, S., et al., 2017. Heavy metal removal using nanoscale zero-valent iron (nZVI): Theory and application. J Hazard Mater 322 (Pt A), 163–171.

[26] Ayalew, Z.M., Guo, X., Zhang, X., 2022. Synthesis and application of polyethyleneimine (PEI)-based composite/nanocomposite material for heavy metals removal from wastewater: a critical review. J Hazard Mater Adv 8.

[27] Wang, F., et al., 2021. Novel polyethyleneimine/κ-carrageenan composite from facile one-step fabrication for the removal of copper ion from aqueous solution. J Polym Environ 30 (3), 1001–1011.

[28] Daniel-da-Silva, A.L., et al., 2012. Impact of magnetic nanofillers in the swelling and release properties of kappa-carrageenan hydrogel nanocomposites. Carbohydr Polym 87 (1), 328–335.

[29] Gupta, S., et al., 2009. Composition dependent structural modulations in transparent poly(vinyl alcohol) hydrogels. Colloids Surf B Biointerfaces 74 (1), 186–190.

[30] Verma, S.K., et al., 2014. Grafting of N-(hydroxymethyl) acrylamide on to kappa-carrageenan: synthesis, characterization and applications. Carbohydr Polym 102, 590–597.

[31] Eltaweil, A.S., et al., 2021. Zero valent iron nanoparticle-loaded nanobentonite intercalated carboxymethyl chitosan for efficient removal of both anionic and cationic dyes. ACS Omega 6 (9), 6348–6360.

[32] Pacheco, D., et al., 2021. Seaweeds' carbohydrate polymers as plant growth promoters. Carbohydr Polym Technol Appl 2.

[33] Gómez-Ordóñez, E., Rupérez, P., 2011. FTIR-ATR spectroscopy as a tool for polysaccharide identification in edible brown and red seaweeds. Food Hydrocoll 25 (6), 1514–1520.

[34] Xu, R., et al., 2019. Preparing sodium alginate/polyethyleneimine spheres for potential application of killing tumor cells by reducing the concentration of copper ions in the lesions of colon cancer. Materials 12 (9).

[35] Rahmani, Z., Ghaemy, M., Olad, A., 2022. Removal of heavy metals from polluted water using magnetic adsorbent based on κ-carrageenan and N-doped carbon dots. Hydrometallurgy 213.

[36] Kalaiselvi, K., et al., 2023. Adsorption of Pb2+ ions from aqueous solution onto porous kappa-carrageenan/cellulose hydrogels: isotherm and kinetics study. Sustainability 15 (12).

[37] Hasan, M.S., et al., 2020. Enhanced heavy metal removal from synthetic stormwater using nanoscale zerovalent iron–modified biochar. Water, Air, Soil Pollut (5), **231**.

[38] Fu, F., et al., 2013. Insights into environmental remediation of heavy metal and organic pollutants: simultaneous removal of hexavalent chromium and dye from wastewater by zero-valent iron with ligand-enhanced reactivity. Chem Eng J 232, 534–540.

[39] Zhu, F., et al., 2022. Efficiency assessment of ZVI-based media as fillers in permeable reactive barrier for multiple heavy metal-contaminated groundwater remediation. J Hazard Mater 424 (Pt C), 127605.

[40] Xu, C., et al., 2018. Performance and mechanism of Cr(VI) removal by zero-valent iron loaded onto expanded graphite. J Environ Sci 67, 14–22.

[41] Sabbagh, F., Khatir, N.M., Kiarostami, K., 2023. Synthesis and characterization of k-carrageenan/PVA nanocomposite hydrogels in combination with MgZnO nanoparticles to evaluate the catechin release. Polymer 15 (2).

[42] Tang, H., et al., 2021. Recent advances in nanoscale zero-valent iron-based materials: characteristics, environmental remediation and challenges. J Clean Prod 319.

[43] L. S. Silva, L., et al., 2019. Evaluation of nano zero-valent iron (nZVI) activity in solution and immobilized in hydrophilic PVDF membrane for drimaren red X-6BN and bisphenol-a removal in water. Processes 7 (12).

[44] Anang, E., Liu, H., Fan, X., 2023. An insight into the fate of Cu2+ and zero-valent iron during removal of Cu2+ by nanoscale zero-valent iron. Water Emerg Contam Nanoplastics 1 (1).

[45] Ji, C., Meng, L., Wang, H., 2019. Enhanced reductive dechlorination of 1,1,1-trichloroethane using zero-valent iron-biochar-carrageenan microspheres: preparation and microcosm study. Environ Sci Pollut Res Int 26 (30), 30584–30595.

[46] Saputri, A.E., et al., *Mechanical and solubility properties of bio-nanocomposite film of semi refined kappa carrageenan/ZnO nanoparticles*. 2018.

[47] Azizi, S., et al., 2017. Hydrogel beads bio-nanocomposite based on Kappa-Carrageenan and green synthesized silver nanoparticles for biomedical applications. Int J Biol Macromol 104 (Pt A), 423–431.

[48] Dogaru, B.I., Simionescu, B., Popescu, M.C., 2020. Synthesis and characterization of kappa-carrageenan bio-nanocomposite films reinforced with bentonite nanoclay. Int J Biol Macromol 154, 9–17.

[49] Ahmed, M.F., et al., 2021. Hybrid beads of zero valent iron oxide nanoparticles and chitosan for removal of arsenic in contaminated water. Water 13 (20).

[50] Alam, J., et al., 2019. k-Carrageenan – A versatile biopolymer for the preparation of a hydrophilic PVDF composite membrane. Eur Polym J 120.
[51] Chen, Z., et al., 2023. Preparation of polyethyleneimine-modified chitosan/Ce-UIO-66 composite hydrogel for the adsorption of methyl orange. Carbohydr Polym 299, 120079.
[52] Yew, H.-C., Misran, M., 2016. Preparation and characterization of pH dependent κ-carrageenan-chitosan nanoparticle as potential slow release delivery carrier. Iran Polym J 25 (12), 1037–1046.
[53] Breite, D., et al., 2016. The critical zeta potential of polymer membranes: how electrolytes impact membrane fouling. RSC Adv 6 (100), 98180–98189.
[54] Karbassiyazdi, E., et al., 2023. Fabrication of carbon-based hydrogel membrane for landfill leachate wastewater treatment. Desalination 564.
[55] Hilliou, L., et al., 2012. The impact of seaweed life phase and postharvest storage duration on the chemical and rheological properties of hybrid carrageenans isolated from Portuguese Mastocarpus stellatus. Carbohydr Polym 87 (4), 2655–2663.
[56] Rhein-Knudsen, N., et al., 2017. Rheological properties of agar and carrageenan from Ghanaian red seaweeds. Food Hydrocoll 63, 50–58.
[57] Yadav, S., et al., 2020. Feasibility of brackish water and landfill leachate treatment by GO/MoS(2)-PVA composite membranes. Sci Total Environ 745, 141088.
[58] Kulal, P., Badalamoole, V., 2020. Hybrid nanocomposite of kappa-carrageenan and magnetite as adsorbent material for water purification. Int J Biol Macromol 165 (Pt A), 542–553.
[59] Azzam, A.M., et al., 2016. Removal of Pb, Cd, Cu and Ni from aqueous solution using nano scale zero valent iron particles. J Environ Chem Eng 4 (2), 2196–2206.
[60] Wu, Y., et al., 2020. Zero-valent iron-based technologies for removal of heavy metal(loid)s and organic pollutants from the aquatic environment: Recent advances and perspectives. J Clean Prod 277.
[61] Tarekegn, M.M., Hiruy, A.M., Dekebo, A.H., 2021. Nano zero valent iron (nZVI) particles for the removal of heavy metals (Cd(2+), Cu(2+) and Pb(2+)) from aqueous solutions. RSC Adv 11 (30), 18539–18551.
[62] Ken, D.S., Sinha, A., 2020. recent developments in surface modification of nano zero-valent iron (nzvi): remediation, toxicity and environmental impacts. Environmental nanotechnology. Monit Manag **14**.
[63] Cai, R., et al., 2023. A self-supported sodium alginate composite hydrogel membrane and its performance in filtering heavy metal ions. Carbohydr Polym 300, 120278.
[64] Amiri, S., et al., 2021. Fabrication of chitosan-aminopropylsilane graphene oxide nanocomposite hydrogel embedded PES membrane for improved filtration performance and lead separation. J Environ Manag 294.
[65] Karbassiyazdi, E., et al., 2023. Gravity-driven composite cellulose acetate/activated carbon aluminium-based hydrogel membrane for landfill wastewater treatment. Chem Eng Res Des 200, 682–692.
[66] Cai, R., et al., 2022. A novel sodium alginate/cellulose nanofiber self-supported hydrogel membrane and its filtration performance. J Water Process Eng 50.
[67] Yang, B., et al., 2021. Chitosan nanofiltration membranes with gradient cross-linking and improved mechanical performance for the removal of divalent salts and heavy metal ions. Desalination 516.
[68] Zhang, X., et al., 2015. A free-standing calcium alginate/polyacrylamide hydrogel nanofiltration membrane with high anti-fouling performance: Preparation and characterization. Desalination 365, 234–241.
[69] Gao, N., et al., 2024. Ba2+ /Ca2+ co-crosslinked alginate hydrogel filtration membrane with high strength, high flux and stability for dye/salt separation. Chin Chem Lett 35 (5).
[70] Hu, J., et al., 2020. A self-supported gel filter membrane for dye removal with high anti-fouling and water flux performance. Polymer 201.
[71] Cai, R., et al., 2024. Self-supported hydrogel loose nanofiltration membrane for dye/salt separation. Sep Purif Technol 328.
[72] Ye, S., et al., 2024. Application and mechanism of lithium-ion sieves in the recovery of lithium-containing wastewater: a review. Water, Air, Soil Pollut 235 (5).